International Journal of Thermofluids 22 (2024) 100690

Contents lists available at ScienceDirect

International Journal of Thermofluids

journal homepage: www.sciencedirect.com/journal/international-journal-of-thermofluids

# Optimizing membrane reactor structures for enhanced hydrogen yield in $CH_4$ tri-reforming: Insights from sensitivity analysis and machine learning approaches

Mohammadali Nasrabadi [a], Agus Dwi Anggono [b,*], Lidia Sergeevna Budovich [c], Sherzod Abdullaev [d,e], Serikzhan Opakhai [f]

[a] Department of Mechanical and Materials Engineering, University of Nebraska-Lincoln, Lincoln, NE, 68588, USA
[b] Mechanical Engineering, Universitas Muhammadiyah Surakarta, Jl. Ahmad Yani PO.BOX 1 Surakarta, Indonesia
[c] MIREA - Russian Technological University (RTU MIREA), 78 Vernadsky Avenue, Moscow, 119454, Russia
[d] Faculty of Chemical Engineering, New Uzbekistan University, Tashkent, Uzbekistan
[e] Scientific and Innovation Department, Tashkent State Pedagogical University named after Nizami, Tashkent, Uzbekistan
[f] Faculty of Physics and Technical science, L.N. Gumilyov Eurasian National University, Astana, 010000, Kazakhstan

ARTICLE INFO

*Keywords:*
$CH_4$ reforming process
Hydrogen production
Membrane reactor
Optimization
Synthesis gas

ABSTRACT

This study explores the optimization of membrane reactor configurations to enhance hydrogen production through $CH_4$ tri-reforming. The investigation employs ceramic membranes for oxygen, vapor, and carbon dioxide distribution within the reactor bed. A differential evolution algorithm is utilized alongside cuckoo search algorithm (CSA) and support vector regression (SVR) to determine optimal values for $O_2/CH_4$, $H_2O/CH_4$, and $CO_2/CH_4$ ratios, membrane thickness, and shell pressure, with hydrogen yield as the objective function. Results demonstrate that the oxygen membrane reactor achieves the highest hydrogen yield, reaching 2.02 and 1.75 for direct methanol synthesis and Fischer–Tropsch processes, respectively, representing a 7.98 % and 10.03 % increase compared to the conventional tri-reforming reactor. Furthermore, CSA and SVR emerge as invaluable tools, facilitating robust optimization and predictive modeling. The CSA efficiently navigates complex solution spaces to identify optimal parameters, while SVR accurately models relationships between input variables and hydrogen yield. Incorporating these methodologies enhances the effectiveness of membrane reactor design and synthesis gas production. This study contributes to advancements in clean energy technologies by providing insights into efficient hydrogen production methods using membrane reactors.

## 1. Introduction

Hydrogen ($H_2$) holds immense significance as a clean and sustainable energy carrier across various sectors, including industrial processes, transportation, and energy storage. One of its primary advantages is its ability to produce energy with zero emissions of greenhouse gases or pollutants when used in fuel cells, making it a crucial component in efforts to combat climate change and transition towards a low-carbon economy [1]. In industrial processes, hydrogen plays a vital role as a feedstock for chemical production, including the synthesis of ammonia, methanol, and various other important chemicals. These processes traditionally rely on fossil fuels, such as natural gas or coal, which generate significant carbon emissions. By using hydrogen produced from renewable sources or low-carbon methods, such as electrolysis powered by renewable electricity or steam reforming with carbon capture and storage (CCS), these industrial processes can significantly reduce their carbon footprint [2]. Moreover, hydrogen's versatility extends to transportation, where it can be used as a fuel for fuel cell electric vehicles (FCEVs) or blended with natural gas for use in internal combustion engines. FCEVs offer zero-emission transportation, emitting only water vapor and heat, making them a promising solution for reducing emissions from the transportation sector, which is a major contributor to air pollution and greenhouse gas emissions [3]. In addition to industrial processes and transportation, hydrogen also serves as a crucial component of energy storage solutions, particularly for integrating renewable energy sources like wind and solar power into the grid. Excess renewable

* Corresponding author.
*E-mail address:* ada126@ums.ac.id (A.D. Anggono).

https://doi.org/10.1016/j.ijft.2024.100690

Available online 9 May 2024

energy can be used to produce hydrogen through electrolysis, which can then be stored and later converted back into electricity through fuel cells or gas turbines when needed. This enables grid operators to manage fluctuations in renewable energy generation and ensure grid stability, facilitating the transition towards a more renewable-based energy system [4]. The growing global interest in hydrogen is evident in the increasing investments, research efforts, and policy initiatives focused on advancing hydrogen technologies and infrastructure. Governments, industries, and research institutions worldwide are recognizing hydrogen's potential to decarbonize various sectors and play a crucial role in achieving climate goals outlined in international agreements like the Paris Agreement [5]. Overall, hydrogen's clean and sustainable attributes make it a key element in transitioning towards a low-carbon economy, offering solutions to address climate change, reduce air pollution, and enhance energy security. As such, harnessing the full potential of hydrogen as an energy carrier is essential for achieving a more sustainable and environmentally friendly future.

The concept of $CH_4$ tri-reforming represents a significant advancement in the field of chemical engineering, particularly in the production of synthesis gas (syngas), a crucial intermediate used in a multitude of industrial processes [6]. $CH_4$ tri-reforming involves the simultaneous conversion of methane ($CH_4$) along with vapor ($H_2O$) and carbon dioxide ($CO_2$) over a catalyst, resulting in the generation of syngas [7]. Syngas is a versatile feedstock widely utilized in numerous industrial applications, including the production of ammonia, methanol, Fischer–Tropsch liquids, and hydrogen [8]. It serves as a precursor for various chemical synthesis processes and holds immense importance in the production of fuels, chemicals, and materials [9]. The significance of $CH_4$ tri-reforming lies in its ability to harness multiple feedstocks, namely CH4, vapor, and carbon dioxide, to produce syngas in a single-step process [10]. This not only simplifies the overall production process but also offers several advantages, including improved process efficiency, reduced energy consumption, and lower greenhouse gas emissions [11]. Furthermore, $CH_4$ tri-reforming facilitates the utilization of abundant and readily available feedstocks such as natural gas and carbon dioxide, thereby contributing to the development of sustainable and environmentally friendly manufacturing processes [12]. By efficiently converting these feedstocks into syngas, $CH_4$ tri-reforming plays a crucial role in meeting the growing demand for clean energy and sustainable chemical production [13]. In summary, $CH_4$ tri-reforming stands as a pivotal process for producing syngas, which serves as a cornerstone in various industrial sectors [14]. Its ability to utilize multiple feedstocks and generate syngas in a single step underscores its importance in advancing sustainable and efficient manufacturing practices [15].

The hydrogen yield plays a pivotal role in synthesizing gas production and subsequent industrial processes due to its versatile applications and importance as a key chemical feedstock [16]. Hydrogen is a fundamental component of syngas, and its availability in sufficient quantities is essential for various industrial applications, including ammonia production, methanol synthesis, Fischer–Tropsch synthesis, and hydrogenation reactions [17]. Optimizing membrane reactor structures to maximize hydrogen yield is paramount for enhancing overall process efficiency and ensuring the economic viability of syngas production [18]. Membrane reactors offer several advantages over traditional reactor configurations, including improved selectivity, enhanced conversion rates, and reduced energy consumption [19]. By integrating membranes into the reactor design, it becomes possible to selectively separate hydrogen from the reaction mixture, thereby increasing its yield and purity [20]. Furthermore, optimizing membrane reactor structures enables better control over reaction conditions, such as temperature and pressure, leading to improved catalyst performance and extended lifespan [21]. This not only enhances hydrogen yield but also contributes to the overall efficiency and sustainability of the syngas production process [18]. Moreover, maximizing hydrogen yield through membrane reactor optimization facilitates downstream processing, as higher-purity hydrogen streams can be obtained, reducing the need for additional purification steps and minimizing energy consumption [22]. This results in cost savings and environmental benefits, making membrane reactor technology a compelling choice for syngas production and subsequent industrial processes [23–25]. In conclusion, optimizing membrane reactor structures to maximize hydrogen yield is crucial for enhancing overall process efficiency, reducing production costs, and promoting sustainable industrial practices [26–28]. Optimizing the membrane reactor structure in $CH_4$ tri-reforming offers several potential advantages, as indicated by the findings outlined in the abstract [22]. These advantages contribute to enhanced process performance compared to conventional reactor designs:

- **Improved $CH_4$ Conversion Rates:** This means that a higher percentage of $CH_4$ molecules can be effectively converted into synthesis gas components, including hydrogen and carbon monoxide [29,30]. Improved $CH_4$ conversion rates increase the overall efficiency of the $CH_4$ tri-reforming process, maximizing the utilization of the $CH_4$ feedstock [31,32].
- **Increased Hydrogen Yield:** One of the primary objectives of optimizing the membrane reactor structure is to maximize hydrogen yield [30,33]. The abstract indicates that under optimal conditions, the oxygen membrane reactor exhibits a significant increase in hydrogen yield compared to conventional reactors [34]. This higher yield of hydrogen is essential for various industrial applications where hydrogen serves as a key chemical feedstock [35]. Increased hydrogen yield not only improves the overall efficiency of syngas production but also reduces the need for additional purification steps [36,37].
- **Extended Catalyst Lifespan:** The elimination of hot spots in the temperature profile, as mentioned in the abstract, helps to mitigate catalyst deactivation and degradation [30,38]. A more uniform temperature distribution within the reactor minimizes thermal stresses on the catalyst, thereby prolonging its effective lifespan [39]. Extended catalyst lifespan reduces the frequency of catalyst replacement or regeneration, leading to cost savings and improved process stability [40,41].
- **Enhanced Process Performance:** Overall, optimizing the membrane reactor structure leads to enhanced process performance compared to conventional reactor designs [42]. The combination of improved $CH_4$ conversion rates, increased hydrogen yield, and extended catalyst lifespan results in a more efficient and sustainable $CH_4$ tri-reforming process [43]. This enhanced performance translates into higher production yields, reduced energy consumption, and lower operating costs, making membrane reactor technology a compelling choice for syngas production in various industrial applications [30,44,45].

Overall, optimizing the membrane reactor structure offers several significant advantages, including improved $CH_4$ conversion rates, increased hydrogen yield, and extended catalyst lifespan [29]. These advantages contribute to enhanced process performance and efficiency, positioning membrane reactors as a promising technology for syngas production in the chemical and energy sectors [46].

The research gap addressed in the introduction of the paper revolves around the optimization of membrane reactor configurations for CH4 tri-reforming. This gap is identified based on the existing challenges and limitations in conventional reactor designs, particularly in achieving high hydrogen yield and efficient synthesis gas production. The novelty of the study lies in proposing innovative approaches to address this gap. Specifically, the introduction highlights the use of a microporous ceramic membrane for oxygen, vapor, and carbon dioxide distribution along the reactor bed, coupled with advanced optimization techniques such as the differential evolution algorithm. Additionally, the integration of machine learning methodologies like the cuckoo search algorithm (CSA) and support vector regression (SVR) represents a novel

aspect of the research, offering powerful capabilities for optimization and predictive modeling in membrane reactor design. Overall, the study aims to fill the research gap by introducing novel membrane reactor configurations and optimization strategies to enhance hydrogen production and synthesis gas generation processes.

The primary objective of this study is to optimize the membrane reactor structure for $CH_4$ tri-reforming. The focus lies in enhancing hydrogen yield to meet the demands of synthesizing gas production for downstream processes. Specifically, the study aims to systematically explore and improve the design of membrane reactors to maximize the production of hydrogen during the $CH_4$ tri-reforming process. By optimizing the membrane reactor structure, we seek to enhance the efficiency and effectiveness of hydrogen production, thereby ensuring an adequate supply of synthesis gas for subsequent industrial processes. The optimization process via CSA involves investigating various factors that influence hydrogen yield, such as reactor configuration, operating conditions, and membrane properties. Through rigorous analysis and experimentation, our goal is to identify the optimal combination of parameters that will lead to the highest possible hydrogen yield in $CH_4$ tri-reforming. Ultimately, by achieving higher hydrogen yields through membrane reactor optimization, we aim to address the increasing demand for synthesis gas in various industrial applications, including ammonia production, methanol synthesis, and hydrocarbon processing. In this case, machine learning technique was used to solve the mentioned issues. This study seeks to contribute to the advancement of sustainable and efficient manufacturing practices by providing insights into optimizing membrane reactor structures for hydrogen production in $CH_4$ tri-reforming processes.

## 2. Methodology

### 2.1. $CH_4$ tri-reforming reactor

The $CH_4$ tri-reforming reactor (conventional reactor) consists of 184 tubes filled with NiO–Mg/Ce–$ZrO_2/Al_2O_3$ catalyst. The dimensions of these catalysts are 16 × 19 and they are of the 10-hole rings type. These catalysts have demonstrated satisfactory performance in reducing coking on the catalyst surface and reactor walls. No external energy is required for the $CH_4$ tri-reforming reactions, and this reactor operates under non-adiabatic conditions [47].

### 2.2. Comparative analysis of membrane CH4 tri-reforming reactor structures

Each tube of the traditional tri-reforming reactor is covered with a non-selective porous ceramic membrane in the membrane $CH_4$ tri-reforming reactor. In this study, three types of membrane reactor structures, namely oxygen membrane reactor, water vapor membrane reactor, and carbon dioxide membrane reactor, are considered. In these three membrane reactor structures, oxygen, water vapor, and carbon dioxide respectively pass through the membrane and are distributed in the catalytic bed. The remaining feed components, apart from the distributed component, enter the catalytic bed from the beginning of the tube.

### 2.3. Mathematical modeling

#### 2.3.1. Kinetic model

Reactions 1 to 4 have been considered to describe the $CH_4$ tri-reforming process [30]:

$$CH_4 + H_2O \leftrightarrow CO + 3H_2 \Delta H_{298} = 206kJ/mol \quad (1)$$

$$CH_4 + 2H_2O \leftrightarrow CO_2 + 4H_2 \Delta H_{298} = 164.9kJ/mol \quad (2)$$

$$CO + H_2O \leftrightarrow CO_2 + H_2 \Delta H_{298} = -41.1kJ/mol \quad (3)$$

$$CH_4 + 2O_2 \leftrightarrow CO_2 + 2H_2O \Delta H_{298} = -802.7kJ/mol \quad (4)$$

The $CH_4$ dry reforming reaction is considered as a non-independent reaction, which can be obtained from the difference between reactions 1 and 3 [48]. Laboratory-scale kinetic equations have been provided for $CH_4$ reforming with vapor (reactions 1–3) over a nickel catalyst [49]. Additionally, a model was proposed for the kinetic equation of $CH_4$ oxidation reaction (reaction 4) [50]. Their proposed model was for a palladium catalyst, and equilibrium absorption coefficients were adjusted for a nickel catalyst [51]. The kinetic equations for reactions 1–4 are expressed with Eqs. (5)–(8) respectively [30]:

$$r_1 = \frac{k_1}{P_{H_2}^{2.5}} \left( P_{CH_4} P_{H_2O} - \frac{P_{H_2}^3 P_{CO}}{K_I} \right) \times \frac{1}{\varnothing^2} \quad (5)$$

$$r_2 = \frac{k_2}{P_{H_2}^{3.5}} \left( P_{CH_4} P_{H_2O}^2 - \frac{P_{H_2}^4 P_{CO_2}}{K_{II}} \right) \times \frac{1}{\varnothing^2} \quad (6)$$

$$r_3 = \frac{k_3}{P_{H_2}} \left( P_{CO} P_{H_2O} - \frac{P_{H_2} P_{CO_2}}{K_{III}} \right) \times \frac{1}{\varnothing^2} \quad (7)$$

$$r_4 = \frac{k_{4a} P_{CH_4} P_{O_2}}{\left( 1 + K_{CH_4^C} P_{CH4} + K_{O_2^C} PO_2 \right)^2} \quad (8)$$

The kinetic coefficients of the rate equation can be expressed (Eqs. (10) and (11)) [30,52]:

$$K_i = K_{0i} \exp\left( -\frac{\Delta H_i}{RT} \right); i = CH_4, CO, H_2, H_2O, CH_4^C, O_2^C \quad (9)$$

$$K_n = \exp\left( \frac{A_n}{T_S} \right); n = I, II, III \quad (10)$$

$$K_j = K_{0j} \exp\left( -\frac{E_j}{RT} \right); j = 1, 2, 3, 4a, 4b \quad (11)$$

#### 2.3.2. Mass and energy conservation equations for the solid phase

One-dimensional heterogeneous mathematical modeling has been conducted to obtain the concentration of components and temperature distribution within the catalytic bed, taking into account mass and heat transfer resistances (Eqs. (12) and (13)) [30].

$$a_v k_{gi} C_t \left( y_i^t - y_{is} \right) + \rho_B \sum_{j=1}^{4} \eta_j v_{i,j} r_j = 0 \quad (12)$$

$$a_v h_f (T^t - T_s) + \rho_B \sum_{j=1}^{4} \eta_j r_j (-\Delta H_R)_j = 0 \quad (13)$$

To simplify the model, the following assumptions have been made (Table 1):

It was demonstrated that the results obtained from two-dimensional modeling of CH4 tri-reforming reactor are close to the results obtained from one-dimensional modeling presented [30,47]. This compatibility justifies the use of one-dimensional modeling for optimization purposes to reduce computational time. Therefore, one-dimensional modeling has been used to estimate reactor behavior. Taking the above assumptions into account, a differential element $\Delta z$ along the axis direction has been considered to obtain the mass and energy conservation equations. Mass and energy conservation equations for calculating intra-particle resistance for reactions 1–4 using the dusty gas model have been calculated [30,55,56].

#### 2.3.3. Mass and energy conservation equations for the fluid phase inside the tube

For the component that passes through the membrane in Eqs. (14) and (15), the coefficient $\beta_i$ is taken as 1, while for the remaining

**Table 1**
Assumptions used in mathematical modeling of $CH_4$ tri-reforming process.

| Assumption number | Assumption description | Reference |
|---|---|---|
| 1 | The compressibility factor of the gas at high temperature and feed pressure conditions is 1.0019. | [53] |
| 2 | The dimensionless Peclet number for the inlet feed flow to the reactor is 7451, indicating negligible axial diffusion against convective gas movement. | [53] |
| 3 | All reactors operate under steady-state conditions. | [53] |
| 4 | The porosity of the bed is constant in both radial and axial directions. | [53] |
| 5 | Energy loss in the conventional tri-reforming reactor is neglected, and the reactor is assumed to be insulated. | [53] |
| 6 | Gas leakage from the tube to the shell is neglected due to the positive pressure difference between them. | [53] |
| 7 | The dimensionless Biot number is less than 0.1, so the temperature gradient inside the catalyst is disregarded. | [54] |

components and the traditional tri-reforming reactor, it is taken as 0 [30].

$$\frac{-1}{NA_c}\frac{\partial\left(F_t y_i^t\right)}{\partial z}+a_v k_{gi} C_t\left(y_{is}-y_i^t\right)+4\beta_i\frac{J_i}{D_i}=0 \tag{14}$$

$$\frac{-1}{NA_c}\frac{\partial\left(F_t c_{p,mix} T^t\right)}{\partial z}+a_v h_f\left(T_s-T^t\right)+\frac{4\alpha U}{D_i}\left(T^s-T^t\right)+\frac{4\beta_i}{D_i}\int_{T^s}^{T^t} J_i c_{pi} dT=0 \tag{15}$$

Additionally, the coefficient $\alpha$ in Eq. (15) is 0 for the conventional tri-reforming reactor because the reactor operates under non-adiabatic conditions, and for membrane reactors, it is equal to one due to heat transfer between the tube and shell.

In Eqs. (16) and (17), $N$ is for the number of tubes, and $i$ denotes oxygen, water vapor, and carbon dioxide in each structure[30].

$$\frac{\partial F_i^s}{\partial z}+N\pi D_i J_i=0 \tag{16}$$

$$\frac{\partial\left(F_i^s c_{pi} T^s\right)}{\partial z}+NU\pi D_i\left(T^s-T^t\right)+N\pi D_i\int_{T^s}^{T^t} J_i c_{pi} dT=0 \tag{17}$$

Eqs. (18)–(22) represent the dusty gas model for calculating the permeation rate of the component through the porous membrane [30, 57].

$$J_i=\frac{-1}{RT_m}\left[\frac{D_i^e}{\delta}\left(P_i^t-P_i^s\right)+\frac{B_0}{\delta\mu_i}P_i^s\left(P^t-P^s\right)\right] \tag{18}$$

$$\frac{1}{D_i^e}=\frac{1}{D_{im}}+\frac{1}{D_{i,k}^e} \tag{19}$$

$$D_{i,k}^e=K_0\sqrt{\frac{8RT}{\pi M_i}} \tag{20}$$

$$K_0=\frac{2}{3}r_p\frac{\varepsilon_m}{\tau} \tag{21}$$

$$B_0=\frac{1}{8}r_p^2\frac{\varepsilon_m}{\tau} \tag{22}$$

Typically, mass transfer across porous membranes is based on the Fick and Darcy's law. This idea states that Knudsen diffusion and boundary layer flow are the ways by which the component permeates the membrane. The permeation flux from the membrane to the structure depends on pressure, temperature, and gas properties. In these conditions, the gas permeation rate through the membrane is calculated based on Eq. (18). The coefficient $\frac{B_0}{\delta\mu_i}$ describes the effective permeability variable dependent on gas viscosity, and $D_{i,k}^e$is the Knudsen diffusion coefficient of component $i$ dependent on temperature and molecular mass of the permeating component through the membrane [58].

The pressure drop equation (Eq. (23)) is expressed by the Ergun equation [30,52].

$$\frac{dP^t}{dz}=150\frac{(1-\varepsilon_B)^2\mu u_g}{\varepsilon_B^3 d_p^2}+1.75\frac{(1-\varepsilon_B)u_g u_g{}^2\rho}{\varepsilon_B^3 d_p} \tag{23}$$

Additionally, to complete the modeling, structural equations such as mass and heat transfer coefficients are required, as reported by [52].

### 2.3.4. Boundary conditions

The pressure, composition percentage of components, and feed temperature entering the tube are considered as boundary conditions for the tube section. Additionally, the feed flow rate and temperature of the entering gas to the shell are considered as boundary conditions for the shell section, summarized as follows [30]:

$$\text{at z}=0\begin{cases}\mathrm{F_i^s}=\mathrm{F_{i0}^s} & \mathrm{T^s}=\mathrm{T_0^s};\ \textit{In the shell section}\\ \mathrm{y_i^t}=\mathrm{y_{i0}^t} & \mathrm{T^t}=\mathrm{T_0^t P^t}=\mathrm{P_0^t};\ \textit{In the pipe section}\end{cases} \tag{24}$$

where $i$ corresponds to oxygen, water vapor, and carbon dioxide components in the shell section of oxygen, water vapor, and carbon dioxide membrane reactors, respectively, and to other feed components in the tube section of the reactors.

## 2.4. Optimization

### 2.4.1. CSA

CSA is a nature-inspired optimization algorithm developed by Xin-She Yang and Suash Deb in 2009. It is inspired by the breeding behavior of certain cuckoo species, particularly the common cuckoo, which is known for its brood parasitism strategy. In the algorithm, each cuckoo (solution candidate) represents a potential solution to an optimization problem. These cuckoos lay eggs (new solutions) randomly in the nests of other cuckoos. The fitness of each cuckoo's eggs is evaluated, and the ones with higher fitness have a higher probability of survival and replacing eggs in less fit nests. These mimics the concept of natural selection and the survival of the fittest [59]. Key features of the Cuckoo Search Algorithm include:

- **Levy Flights:** Cuckoos' movement between solutions is modeled using Levy flights, which are random walks with a step size following a Levy distribution. This allows for a balance between local exploitation and global exploration in the search space [60].
- **Randomness:** The algorithm incorporates randomness in the search process, enhancing its ability to explore diverse regions of the solution space [60].
- **Local Search:** Optionally, local search methods can be integrated into the algorithm to refine solutions further [60].

The Cuckoo Search Algorithm has been applied to various optimization problems, including function optimization, parameter estimation, and machine learning. It is known for its simplicity, efficiency, and effectiveness in finding high-quality solutions in both continuous and discrete optimization domains [61].

### 2.4.2. Formulation of the optimization problem

In this study, maximizing hydrogen yield has been considered as the objective function. The hydrogen to carbon monoxide ratio in the outlet gas should be in the range of 1.5–2 for the first condition and 1–1.5 for the second condition because the goal of the current research is to produce synthesis gas suitable for the production of methanol, gas-to-

liquid conversion, and direct synthesis of dimethyl ether. From an environmental perspective, the $CO_2$ conversion in the reactor outlet should not be less than the $CO_2$ conversion in the outlet of the conventional tri-reforming reactor (11.56 %) [52]. Additionally, to prevent catalyst deactivation throughout the reactor, the catalyst temperature should not exceed 1700 K [47]. It is important to note that most ceramic membranes melt at temperatures higher than 2000 °C. For this reason, the membrane is not physically harmed by gas temperatures below 1700 K [62]. Generally, the constraints used for optimization are as follows [30]:

$$\begin{cases} 1.5 < H_2/CO < 2 & \textit{Gas to liquid conversion for synthesis unit} \\ 1 < H_2/CO < 1.2 & \textit{Direct dimethyl ether} \end{cases} \quad (25)$$

$$CO_2 > 11.56\% \quad (26)$$

$$T_s < 1700\,K \quad (27)$$

To solve the optimization problem, machine learning techniques can also be used for this purpose, particularly in the context of optimization problems with complex or nonlinear objective functions and constraints. In this case, neural architecture search techniques use machine learning algorithms to automatically search for optimal neural network architectures with respect to a given objective function, such as model accuracy or computational efficiency.

Support vector regression (SVR) is effective for regression tasks, especially when dealing with datasets with high dimensionality or nonlinearity. It handles both linear and nonlinear relationships and is robust to outliers.

#### 2.4.3. SVR

SVR, which is a type of supervised learning algorithm used for regression tasks. It is an extension of Support Vector Machines (SVMs), which are primarily used for classification. In SVR, the algorithm aims to find a function that best fits the training data while also controlling for error. It works by mapping the input data into a higher-dimensional feature space using a kernel function and then finding the hyperplane that best separates the data points. Unlike traditional regression models that aim to minimize error, SVR aims to ensure that the error falls within a specified tolerance level (controlled by a parameter called epsilon), while still maximizing the margin between the data points and the regression line. Key components of SVR include:

- **Kernel Trick:** SVR uses a kernel function to transform the input data into a higher-dimensional space. This allows SVR to handle nonlinear relationships between the input variables and the target variable.
- **Margin:** SVR aims to find a hyperplane that has a maximum margin from the closest data points (support vectors) while still fitting the data within a specified tolerance level.
- **Regularization:** SVR uses regularization parameters to control the trade-off between maximizing the margin and minimizing the error on the training data. This helps prevent overfitting and ensures better generalization to unseen data.

Overall, SVR is a powerful algorithm for regression tasks, especially when dealing with datasets with high dimensionality, nonlinearity, and noise. It is widely used in various fields such as finance, engineering, and bioinformatics for tasks like time series prediction, function approximation, and anomaly detection [63].

### 2.5. Efficiency criteria

RMSE (Root Mean Square Error) and $R^2$ (R-squared) are commonly used metrics to evaluate the performance of regression models.

- **RMSE:** RMSE measures the average deviation of the predicted values from the actual values. It is calculated by taking the square root of the mean of the squared differences between the predicted values ($\hat{y}$) and the actual values ($y$).

$$RMSE = \sqrt{\frac{\sum_{i=1}^{n}(y_i - \hat{y}_i)^2}{n}} \quad (28)$$

Where: $n$ is the number of observations. $y_i$ is the actual value for observation $i$. $\hat{y}$ is the predicted value for observation $i$.

- **R-squared ($R^2$):** $R^2$ is a measure of the proportion of variance in the dependent variable ($y$) that is predictable from the independent variables ($X$) in the regression model. It ranges from 0 to 1 and indicates the goodness of fit of the model. A value closer to 1 indicates a better fit.

$$R^2 = 1 - \frac{\sum_{i=1}^{n}(y_i - \hat{y}_i)^2}{\sum_{i=1}^{n}(y_i - \bar{y}_i)^2} \quad (29)$$

Where: $n$ is the number of observations. $y_i$ is the actual value for observation $i$. $\hat{y}$ is the predicted value for observation $i$. $\bar{y}$ is the mean of the actual values.

These metrics are commonly used in regression analysis to assess the accuracy and goodness of fit of the regression model. RMSE provides an absolute measure of the model's performance, while $R^2$ provides a relative measure of how well the model explains the variability in the dependent variable [64].

## 3. Results and discussions

### 3.1. Reference state

A reference state is considered as a benchmark for assessing the behavior of various reactor structures. According to the previous study [47], the molar ratios of feed components, such as carbon dioxide/-methane ratio is 1.33, carbon monoxide/methane ratio is 0.00053, hydrogen/methane ratio is 0.082, oxygen/methane ratio is 0.47, nitrogen/methane ratio is 0.00053, and water/methane ratio is 2.47. These ratios determine the composition of the feed entering the reactor. Additionally, the operational conditions are specified, including the input temperature = 1100 K, input pressure = 20 bar, and feed discharge rate = 9129.6 kMol/hr. These conditions are crucial for controlling reaction kinetics and ensuring optimal reactor performance. Furthermore, the dimensions of the reactor components are outlined, including the number of pipes (184), inner pipe diameter (0.125 m), pipe length (2 m), and shell diameter (2.5 m). These dimensions are essential for designing and constructing the reactor to accommodate the specified feed flow rates and operating conditions effectively.

The ceramic membrane used in all three reactor structures is made of alpha-alumina with a pore diameter of $9.3 \times 10^{-8}$ m and a tortuosity ratio of 0.3. According to the study [58], it is possible for various components such as hydrogen, helium, oxygen, carbon dioxide, and propane to permeate through this membrane. Therefore, this type of porous membrane is suitable for permeation of the components under study in this research. The characteristics of such membranes include high permeability, thermal stability, and chemical stability. In the reference conditions, the shell pressure is considered to be 24 bar.

The distribution of gas temperature and the molar discharge (flow) rates of chemical components are derived for the oxygen membrane reactor, carbon dioxide membrane reactor, vapor membrane reactor, and conventional reactor by applying SVR along the reactor bed. Additionally, the hydrogen-to-carbon monoxide ratio, CH4 and carbon dioxide conversions, and hydrogen yield are defined to describe the

reactor performance as follows (Eqs. (28)–(31)) [30]:

$$H_2 \Big/ CO\ Ratio = \frac{F_{H_2}}{F_{CO}} \tag{30}$$

$$CO_2\ Conversion\ Rate = \frac{F_{CO_{2,0}} - F_{CO_2}}{F_{CO_{2,0}}} \tag{31}$$

$$CH_4\ Conversion\ Rate = \frac{F_{CH_{4,0}} - F_{CH_4}}{F_{CH_{4,0}}} \tag{32}$$

$$Hydrogen\ Yield = \frac{F_{H_2} - F_{H_{2,0}}}{F_{CH_{4,0}}} \tag{33}$$

### 3.2. Validation

The obtained results of simulation process were cross-referenced with empirical dataset for CH4 tri-reforming, conducted under specific conditions: molar feed ratios of $CH_4$:$CO_2$:$O_2$:$H_2O$ = 1:1:0.1:1, Gas Hourly Space Velocity (GHSV) = 10,000 $h^{-1}$, and an inner tube diameter of 7 mm utilizing a nickel catalyst. This comparison aimed to validate the accuracy of the provided mathematical model. Analysis, as presented in Table 2, demonstrates a favorable concordance between the simulated outcomes and experimental observations [65].

Therefore, the mathematical model presented can be used for simulating both membrane reactors and conventional reactors. Our study's findings were subjected to comparison with those of previous research endeavors in the field [30], revealing a notable level of compatibility. The outcomes obtained through our investigation align closely with the conclusions drawn from prior studies, affirming the robustness and reliability of our experimental approach and analytical methodologies. This consistency across multiple studies underscores the validity and reproducibility of our results, further reinforcing the significance and relevance of our research findings in the broader scientific community.

### 3.3. Sensitivity analysis

This section looks at the effects of several factors on hydrogen yield and the hydrogen-to-carbon monoxide ratio under baseline circumstances. These variables include shell pressure, membrane thickness, and the molar flow rate of feed components. Then, a comparison is made between different feed structures under optimal conditions with the same molar flow rate of $CH_4$ at the inlet. In the conducted study, sensitivity analysis played a pivotal role in elucidating the influence of various operational parameters on reactor performance. Through meticulous examination, the sensitivity analysis aimed to identify key factors affecting the system's behavior and assess their relative importance. Specifically, factors such as the ratios of $O_2/CH_4$, $H_2O/CH_4$, and $CO_2/CH_4$, membrane thickness, and shell pressure were scrutinized to understand their impact on hydrogen yield, which served as the objective function for optimization.

The utilization of sensitivity analysis allowed for a comprehensive evaluation of how changes in these parameters affected reactor performance, providing valuable insights for process optimization and design refinement. By systematically varying each parameter while keeping others constant, researchers were able to quantify their individual contributions to hydrogen yield and identify potential areas for improvement. Moreover, sensitivity analysis facilitated the identification of optimal operating conditions by highlighting the parameters with the most significant influence on reactor performance. This information guided the subsequent optimization process, enabling researchers to focus their efforts on adjusting key parameters to maximize hydrogen yield while minimizing resource consumption and operational costs. Overall, sensitivity analysis served as a fundamental tool for understanding the complex interactions within the reactor system and guiding decision-making processes towards optimal design and operation. Through systematic exploration of parameter sensitivities, researchers gained valuable insights into the underlying mechanisms governing reactor performance, paving the way for enhanced efficiency, sustainability, and economic viability of membrane reactor systems for hydrogen production and synthesis gas generation.

### 3.4. Impact of various variables on hydrogen yield

In this section, we delve into the influence of molar flow rates of feed components within the tube on hydrogen yield within membrane reactors. Illustrated in Fig. 1a, we observe the correlation between hydrogen yield at the outlet of the oxygen membrane reactor and varying $H_2O/CH_4$ and $CO_2/CH_4$ ratios. Notably, as the $H_2O/CH_4$ ratio escalates from 1 to 3, there's a corresponding increase in hydrogen yield. This augmentation is ascribed to the heightened hydrogen yield witnessed in reactions 1–3, propelled by an upsurge in water vapor content within the reactor. Further elucidating this phenomenon, Fig. 1b portrays the distribution of hydrogen molar discharge (flow) rates along the reactor across various water/methane ratios. We discern a vertical shift in the distribution of hydrogen molar flow rate with escalating water vapor content. Conversely, Fig. 1a depicts a decline in hydrogen yield with an increase in the $CO_2/CH_4$ ratio. This downturn is attributed to the water–gas shift reaction's sensitivity to variations in carbon dioxide concentration. This trend is also apparent in Fig. 1c, where an uptick in carbon dioxide content results in a downward shift in the distribution of hydrogen molar flow rates. Fig. 1b and c collectively demonstrate the rapid increase in hydrogen molar flow rate within the initial reactor segment due to hydrogen production from vapor $CH_4$ reforming reactions. Subsequently, the hydrogen flow rate gradually ascends owing to a reduction in $CH_4$ reforming reaction rates, consequent to a decline in $CH_4$ concentration within the reactor.

Fig. 2a delineates the impact of oxygen/methane and carbon-dioxide/methane ratios on hydrogen yield at the outlet of the vapor membrane reactor. Given the endothermic nature of vapor $CH_4$ reforming reactions, augmenting the $O_2/CH_4$ ratio and gas temperature via complete oxidation of $CH_4$ (reaction 4) leads to increased reaction rates and hydrogen production. However, the predominance of complete $CH_4$ oxidation over vapor $CH_4$ reforming reactions, coupled with a more pronounced water–gas shift reaction at higher temperatures, precipitates a subsequent decline in hydrogen yield. For a more nuanced understanding, the hydrogen molar discharge (flow) rate distribution along the bed at varying oxygen/methane ratios is depicted in Fig. 2b. Here, within the initial reactor, the hydrogen molar flow rate

**Table 2**
Comparison of simulation results and reported laboratory data for $CH_4$ tri-reforming reactor.

| Variable | Feed temp. | | | Feed temp. | | |
|---|---|---|---|---|---|---|
| | 1023 K | | | 1123 K | | |
| | Lab data | Simulation results | Error (%) | Lab data | Simulation results | Error (%) |
| $CH_4$ Conversion Rate | 98.10 | 98.69 | 0.59 | 99.85 | 99.91 | 0.06 |
| Mol of $CO_2$ (%) | 12.93 | 13.23 | 0.30 | 10.81 | 10.85 | 0.04 |
| Mol of CO (%) | 30.72 | 30.33 | 0.39 | 33.89 | 33.98 | 0.09 |
| Mol of $H_2$ (%) | 54.29 | 54.81 | 0.52 | 55.03 | 55.06 | 0.03 |

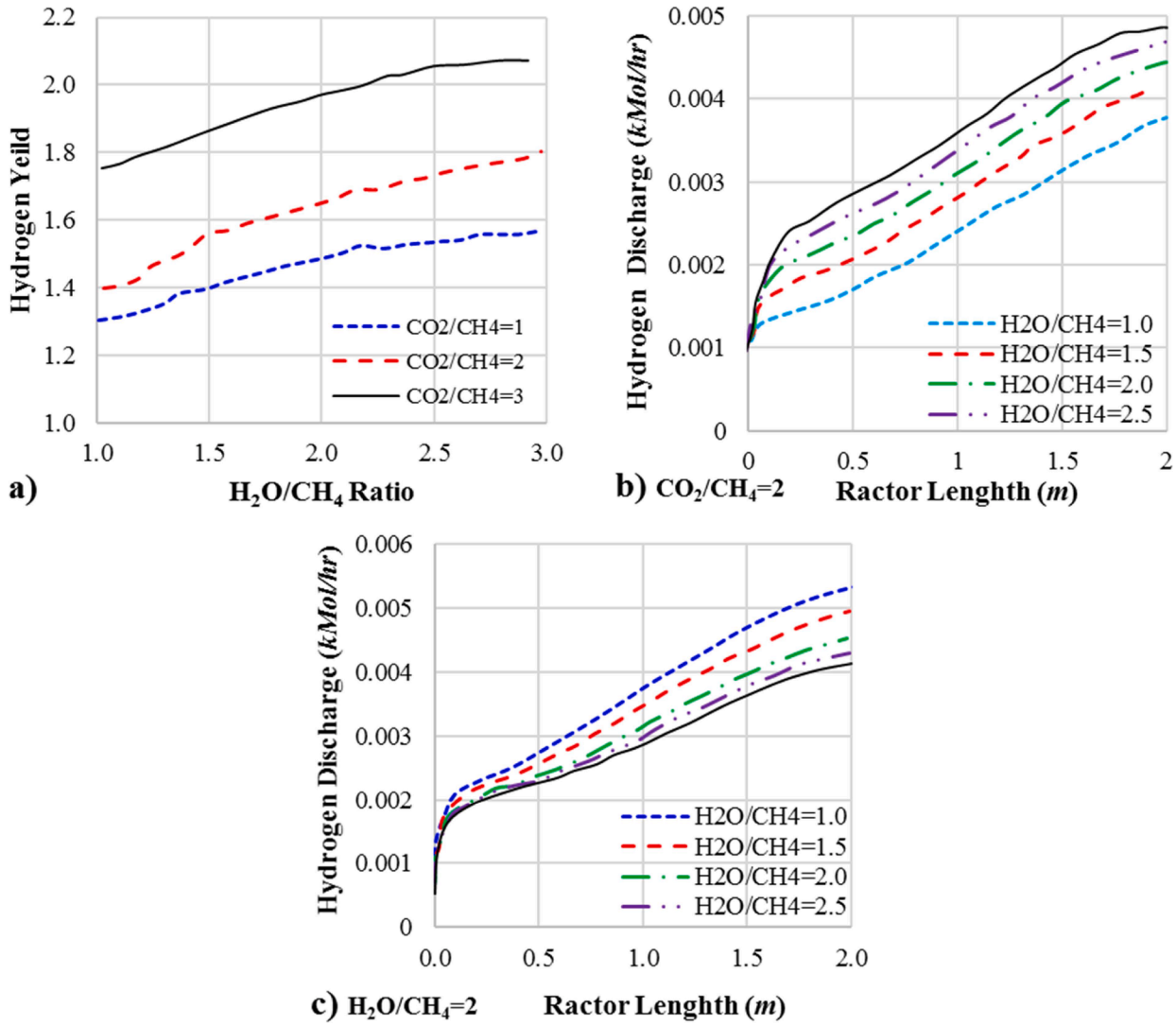


**Fig. 1.** a. Impact of $H_2O/CH_4$ & $CO_2/CH_4$ on the hydrogen yield in the oxygen membrane reactor b. Impact of $H_2O/CH_4$ on the hydrogen mol discharge in the oxygen membrane reactor c. Impact of $CO_2/CH_4$ on the hydrogen mol discharge in the oxygen membrane reactor.

experiences an upward trajectory due to vapor $CH_4$ reforming reactions triggered by an increase in the oxygen/methane ratio. Additionally, an ascending trend is evident within the $O_2/CH_4$ ratio range of 0.1–0.5, succeeded by a declining trend for ratios exceeding 0.5. This behavior stems from the complete oxidation of $CH_4$ reaction and the water–gas shift reaction. Notably, augmenting the $O_2/CH_4$ ratio beyond 0.8 exerts minimal impact on hydrogen yield. Optimal hydrogen yield is attained at varied $CO_2/CH_4$ ratios, approximately around 0.45. The decline in hydrogen yield with increasing $CO_2/CH_4$ ratio (as depicted in Fig. 2a) mirrors the aforementioned reasons for the oxygen membrane reactor. To illustrate, Fig. 2c portrays the distribution profile of the hydrogen molar flow rate at various $CO_2/CH_4$ ratios, showcasing a downward shift with escalating ratios.

Fig. 3a depicts the impact of $O_2/CH_4$ and $H_2O/CH_4$ ratios on hydrogen yield in the carbon dioxide membrane reactor. Initially, the hydrogen yield increases with an increment in the $O_2/CH_4$ ratio and then decreases. A reduction in the $H_2O/CH_4$ ratio from 3 to 1 leads to a decrease in hydrogen yield and shifts the maximum point towards the right. For a better understanding of Fig. 3a, the distribution of hydrogen flow intensity at various $H_2O/CH_4$ and $O_2/CH_4$ ratios along the catalyst bed of the carbon dioxide membrane reactor is plotted in Fig. 3b and c, respectively.

In the initial phase within the reactor, reforming reactions prompt a rapid surge in hydrogen flow intensity, reaching a peak. Subsequently, with the distribution of carbon dioxide throughout the bed facilitated by the membrane and the ascension of the water–gas shift reaction to prominence, a declining trend ensues in the distribution of hydrogen flow intensity within the bed. As depicted in Fig. 3b, as the oxygen/methane ratio escalates from 0.1 to 0.5, the apex of the hydrogen molar discharge (flow) rate distribution shifts upwards, signifying heightened $H_2$ generation (production) attributed to reforming reactions. However, the zenith of the hydrogen molar flow rate distribution later descends, indicative of a diminished contribution from $CH_4$ reforming processes compared to total $CH_4$ oxidation. Similarly, as illustrated in Fig. 3c, an increase in the $H_2O/CH_4$ ratio prompts an upward shift in the distribution of hydrogen molar flow rate, underscoring heightened rates of reforming reactions with an augmented presence of water vapor as a reactant. Moreover, alterations in the pressure differential between the shell and the tube impact the rate at which components permeate the membrane. Specifically, widening the pressure differential amplifies the rate at which components penetrate the membrane, while thickening the membrane exerts the opposite effect. Elevating the shell pressure and reducing the membrane thickness substantially augment the permeate flow rate of components across the membrane.

Fig. 4a illustrates the impact of membrane thickness and shell pressure on hydrogen yield within membrane reactors. In the oxygen

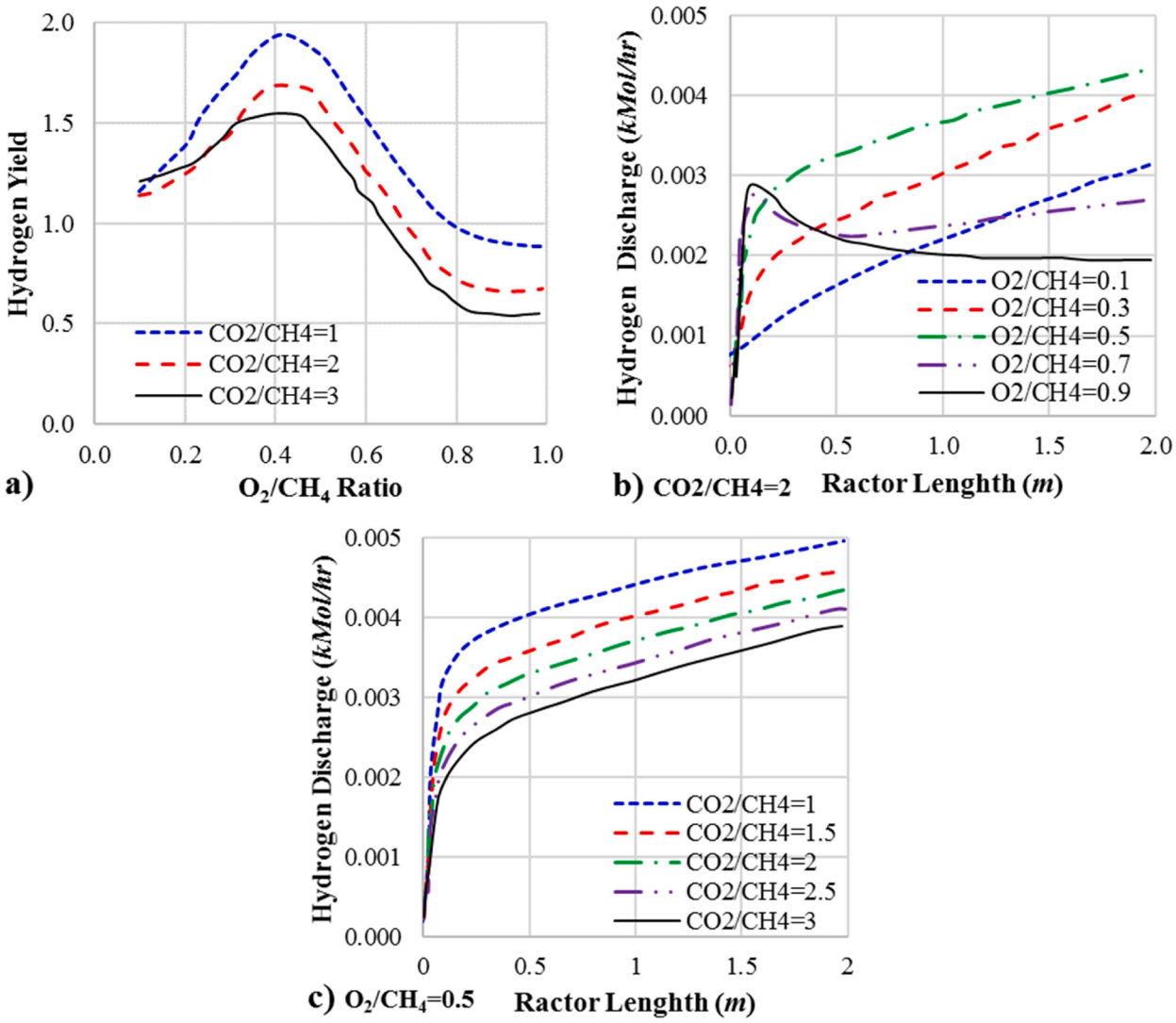


**Fig. 2.** a. Impact of $O_2/CH_4$ & $CO_2/CH_4$ on the hydrogen yield in the vapor membrane reactor b. Impact of $O_2/CH_4$ on the hydrogen mol discharge in the vapor membrane reactor c. Impact of $CO_2/CH_4$ on the hydrogen mol discharge in the vapor membrane reactor.

membrane reactor, reducing membrane thickness at a fixed shell pressure facilitates greater oxygen permeation, consequently amplifying hydrogen production through CH4 reforming reactions, as depicted in Fig. 4a. Subsequently, as reforming processes contribute less relative to full $CH_4$ oxidation, hydrogen output initiates a decline. An elevation in shell pressure from 21 to 25 bar shifts the peak hydrogen yield point towards the right. In Fig. 4b, augmenting vapor permeate flow rate under high pressures and low membrane thicknesses within the vapor membrane reactor results in heightened hydrogen yield attributable to the progression of $CH_4$ reforming reactions and gas-water transfer. Conversely, Fig. 4c reveals a divergent pattern for the carbon dioxide membrane reactor compared to the vapor membrane reactor; at elevated shell pressures and reduced membrane thicknesses, hydrogen yield diminishes due to escalated carbon dioxide concentration. This surge in carbon dioxide concentration prompts greater hydrogen consumption owing to enhanced gas-water transfer reactions. Moreover, extending the membrane thickness beyond 1.5 mm demonstrates minimal impact on hydrogen production, as evidenced by Fig. 4b and c.

It is noteworthy to mention that the plots generated from our study were meticulously compared to those obtained in previous research endeavors, revealing a remarkable level of compatibility [30]. Our findings closely mirror the trends and patterns observed in earlier studies, indicating a consistent portrayal of the underlying phenomena across different experimental settings. This alignment with previous works serves to validate the accuracy and reliability of our plotted data, underscoring the robustness of our experimental methods and analytical techniques. Such congruence with existing literature not only corroborates the validity of our results but also enhances the overall credibility of our research outcomes within the scientific community.

### *3.5. The impact of various variables on the hydrogen to carbon monoxide ratio*

This section delves into the factors influencing the hydrogen to carbon monoxide ratio in membrane reactors. Fig. 5a scrutinizes the impact of $H_2O/CH_4$ and $CO_2/CH_4$ ratios on the hydrogen to carbon monoxide ratio in oxygen membrane reactors. An escalation from a $CO_2/CH_4$ ratio of 1–3 prompts advancements in reforming reactions and water–gas shift reactions, consequently elevating the hydrogen to carbon monoxide ratio. Given that the water–gas shift reaction is influenced by carbon dioxide concentration, augmenting the $H_2O/CH_4$ ratio leads to a reduction in the hydrogen to carbon monoxide ratio. In Fig. 5b, a diminishing trend is evident for the hydrogen to carbon monoxide ratio in vapor membrane reactors at lower $O_2/CH_4$ ratios. As expected, Fig. 5c showcases analogous alterations in the hydrogen to carbon monoxide ratio in carbon dioxide membrane reactors relative to increases in $O_2/$

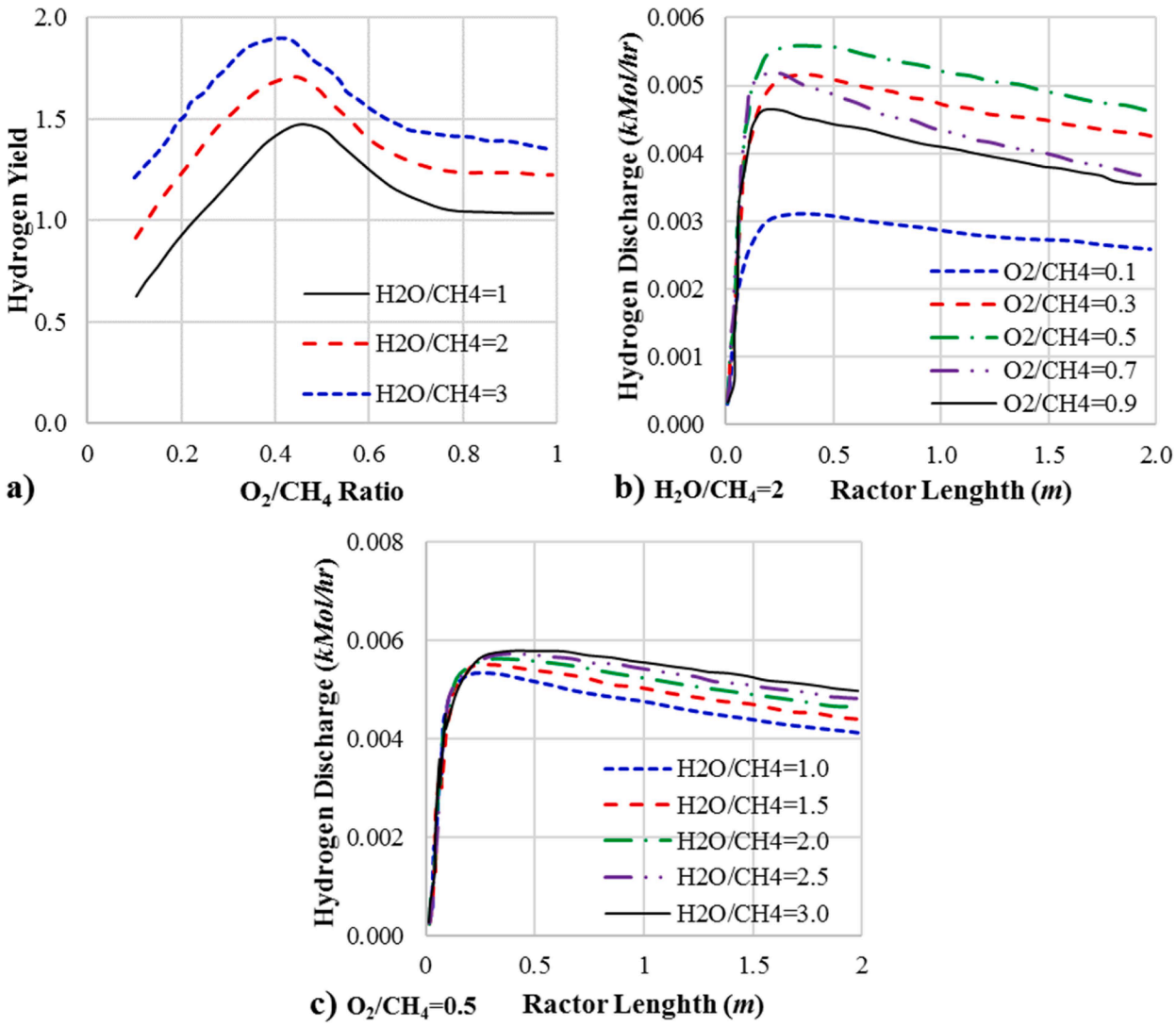


**Fig. 3.** a. Impact of $O_2/CH_4$ & $H_2O/CH_4$ on the hydrogen yield in the carbon dioxide membrane reactor b. Impact of $O_2/CH_4$ on the hydrogen mol discharge in the carbon dioxide membrane reactor c. Impact of $H_2O/CH_4$ on the hydrogen mol discharge in the carbon dioxide membrane reactor.

$CH_4$ and $CO_2/CH_4$ ratios. The reduction in $H_2O/CH_4$ ratio from 3 to 1 induces a shift in the minimum point of the hydrogen to carbon monoxide ratio towards the right.

Fig. 5d demonstrates the changes in the hydrogen to carbon monoxide ratio considering variations in shell pressure and membrane thickness in oxygen membrane reactors. Increasing the oxygen permeation through the membrane enhances the desirability of the complete $CH_4$ oxidation reaction (Reaction 4). Because of the increased activity of the water–gas shift reaction, which consumes hydrogen and produces carbon monoxide, the increment of the shell pressure or reducing the membrane thickness causes the hydrogen to carbon monoxide ratio in oxygen membrane reactors to decrease. As depicted in Fig. 5e, increasing the vapor permeation through the membrane results in an increase in the hydrogen to carbon monoxide ratio in vapor membrane reactors due to the advancement of $CH_4$ reforming reactions. In Fig. 5f, a different trend is observed for the carbon dioxide membrane reactor compared to the vapor membrane reactor. At high shell pressures and low membrane thicknesses, the hydrogen to carbon monoxide ratio decreases due to the increased concentration of carbon dioxide in the reactor, leading to a more active water–gas shift reaction.

The plots generated through the application of our chosen technique were thoroughly compared with those derived from prior studies, revealing a notable consistency across the literature. Our results exhibit a striking resemblance to the trends and patterns documented in earlier research endeavors, affirming the reliability and validity of our methodology [30].

### 3.6. Optimization results

Based on the sensitivity analysis conducted, optimization was performed by selecting the ratios of $CO_2/CH_4$, $H_2O/CH_4$ and $O_2/CH_4$ as well as membrane thickness and using shell pressure as a deciding factor, the goal is to maximize hydrogen output. Since the performance of this method is reliant on the CSA, the objective function is shown depending on the iteration count in Fig. 6, indicating the evolution of outcomes during optimization.

In order to generate synthesis gas suitable for the $CH_3OH$ and Fischer–Tropsch synthesis processes as well as the direct dimethyl ether production process, Table 3 presents the optimal values of decision variables for oxygen, vapor, and carbon dioxide membrane reactors as well as for a conventional reforming reactor.

This table also illustrates the reactor performance, including $CH_4$ and carbon dioxide conversion rates, hydrogen to carbon monoxide ratio, and hydrogen yield, under optimal conditions. Based on the obtained results for the synthesis gas production process suitable for methanol and Fischer–Tropsch synthesis, the oxygen membrane reactor requires

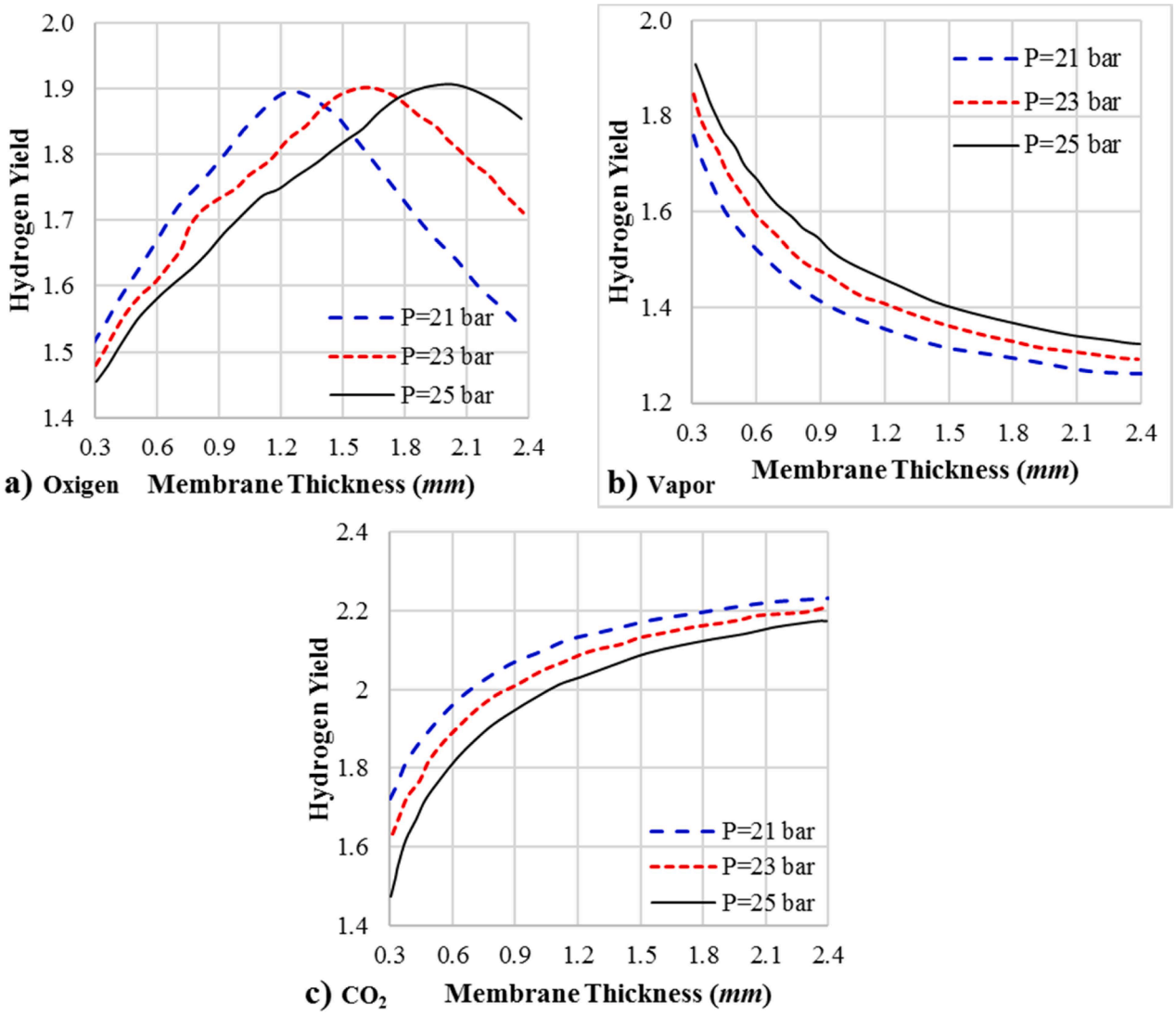


**Fig. 4.** a. Impact of thickness membrane and shell pressure on the hydrogen yield in the oxygen membrane reactor b. Impact of thickness membrane and shell pressure on the hydrogen yield in the vapor membrane reactor c. Impact of thickness membrane and shell pressure on the hydrogen yield in the carbon dioxide membrane reactor.

the highest membrane thickness, the highest ratios of $H_2O/CH_4$ and $O_2/CH_4$, and the highest shell pressure among the reactors. Therefore, the oxygen membrane reactor demands more vapor and oxygen as feed, as well as more energy to increase the pressure in the shell section. This leads to increased operational costs. However, the hydrogen yield in the outlet of the oxygen membrane reactor is 2.03, which is approximately 7.98 % higher than the hydrogen yield of other reactors. The hydrogen to carbon monoxide ratio for all structures ranges from 1.5 to 2, which is suitable for methanol synthesis and the Fischer–Tropsch process. Additionally, the carbon dioxide conversion rate in all reactors is 11.56. These findings were compared to previous research, showing a high level of compatibility [30]. Our outcomes closely match those of earlier studies, confirming the reliability of our experimental and analytical methods. This consistency across studies validates our results and highlights their significance in the scientific community.

The obtained results under optimal conditions for all four reactor structures in the production of synthesis gas suitable for direct dimethyl ether production demonstrate that the oxygen membrane reactor exhibits the highest hydrogen yield, equal to 1.76, $CH_4$ conversion rate of 99.36 %, and carbon dioxide conversion rate of 35.8 %, along with the lowest vapor consumption rate at the reactor inlet compared to other reactors. However, it has the highest membrane thickness, shell pressure, and oxygen consumption among the investigated structures.

Excessive increase in membrane thickness in the oxygen membrane reactor leads to an over-passage of oxygen through the membrane and increased $CH_4$ consumption in the complete oxidation reaction [66]. Consequently, less $CH_4$ remains for vapor reforming reactions, resulting in unsuitable synthesis gas for subsequent processes. This justifies the thicker membrane in the oxygen membrane reactor compared to other membrane reactors [67]. The hydrogen to carbon monoxide ratio is consistent and equal to 1.2 for all structures to achieve the maximum hydrogen yield at the reactor outlet [68].

Reaching a synthesis gas composition characterized by a high $CO/CO_2$ ratio holds significant importance in the effective manufacturing of methanol and dimethyl ether. When the $CO_2/CO$ ratio surpasses a certain threshold, there is a notable increase in both the conversion rate and reaction rate. This phenomenon is primarily attributed to the preferential reactivity of CO over $CO_2$ when in contact with the copper catalyst. Moreover, the reduction in water formation serves to decrease the quantity of water exiting the reactor, consequently mitigating the rate of catalyst deactivation. Consequently, it is evident that the vapor membrane reactor, boasting a $CO_2/CO$ ratio of 1.36, along with the oxygen membrane reactor, featuring a ratio of 2.05, emerge as the optimal reactor configurations for synthesizing gases with heightened

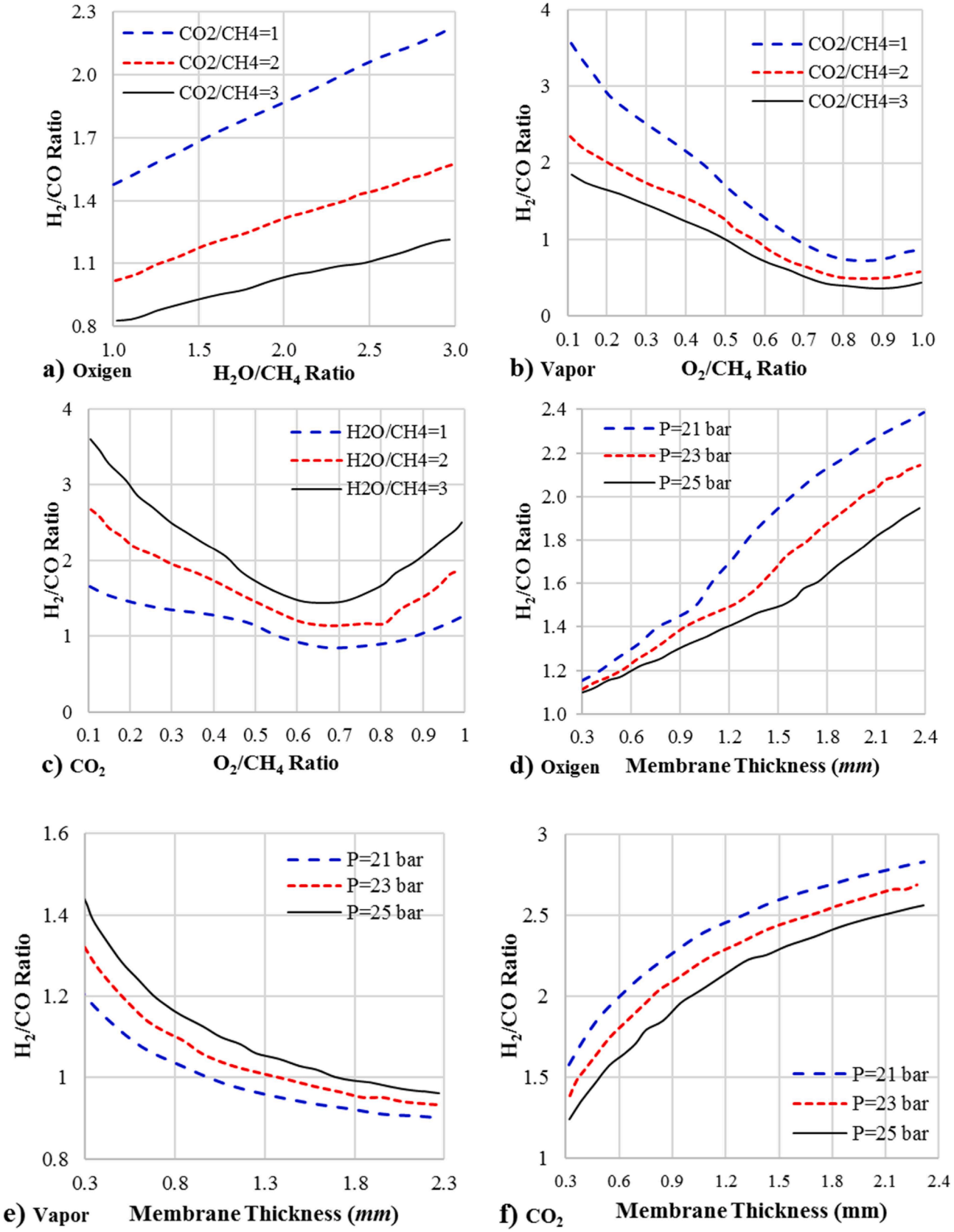


**Fig. 5.** Impact of various ratios, thickness membrane and shell pressure on the $H_2/CO$ in the oxygen, vapor and carbon dioxide membrane reactors.

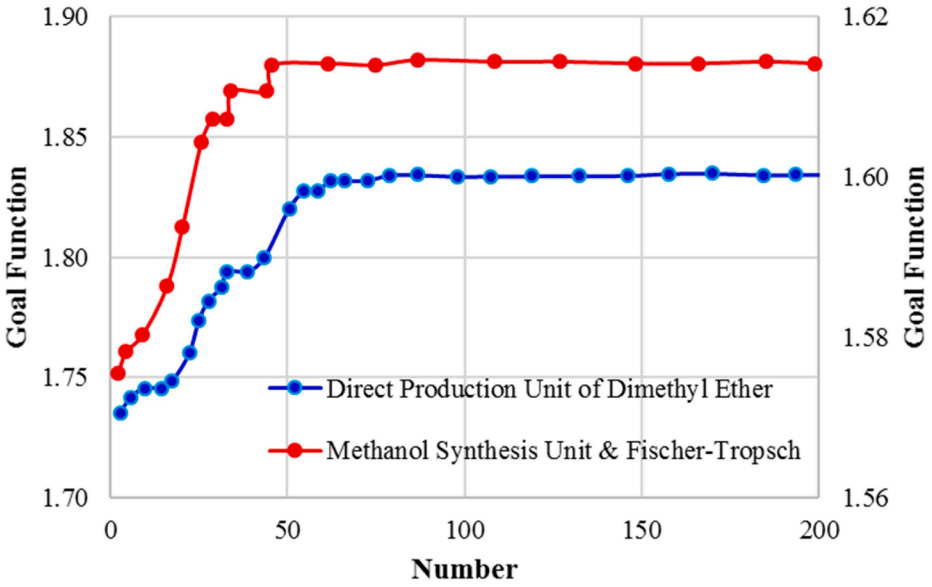


**Fig. 6.** Variations of the objective function vs. the number of counters for the conventional tri-reforming reactor.

**Table 3**
Optimum variables for synthesis gas production, suitable for a) methanol synthesis and Fischer–Tropsch, and b) direct production of dimethyl ether processes.

| Variable | Value | | | | | | | |
|---|---|---|---|---|---|---|---|---|
| | Methanol & Fischer–Tropsch | | | | Direct production unit of dimethyl ether | | | |
| | Conventional | Oxygen | Vapor | Carbon dioxide | Conventional | Oxygen | Vapor | Carbon dioxide |
| $O_2/CH_4$ | 0.45 | 0.57 | 0.45 | 0.45 | 0.43 | 0.59 | 0.49 | 0.45 |
| $H_2O/CH_4$ | 2.03 | 2.36 | 1.98 | 2.16 | 3.5 | 1.04 | 2.76 | 3.48 |
| $CO_2/CH_4$ | 1.01 | 1.01 | 0.88 | 1.01 | 3.7 | 1.19 | 2.51 | 3.82 |
| Shell Pressure (bar) | – | 25 | 21.3 | 21.55 | – | 24.95 | 22.85 | 24.88 |
| Membrane Thickness (mm) | – | 1.73 | 0.32 | 0.54 | – | 1.49 | 0.40 | 0.28 |
| Hydrogen Yield | 1.90 | 2.02 | 1.89 | 1.87 | 1.58 | 1.77 | 1.58 | 1.64 |
| $H_2/CO$ | 1.78 | 1.73 | 1.82 | 1.80 | 1.1 | 1.1 | 1.1 | 1.1 |
| $CO_2$ Conversion (%) | 11.56 | 11.56 | 11.56 | 11.56 | 11.56 | 35.82 | 16.05 | 11.56 |
| $CH_4$ Conversion (%) | 97.86 | 98.33 | 97.39 | 97.6 | 97.89 | 99.38 | 99.78 | 98.29 |
| $CO/CH_2$ | 1.22 | 1.26 | 1.35 | 1.15 | 0.41 | 2.07 | 0.66 | 0.43 |

efficiency in methanol and dimethyl ether production processes.

### 3.7. SVR results

Fig. 7 depicts the distribution of gas temperature and molar discharge (flow) rate along the reactor bed in a membrane reactor

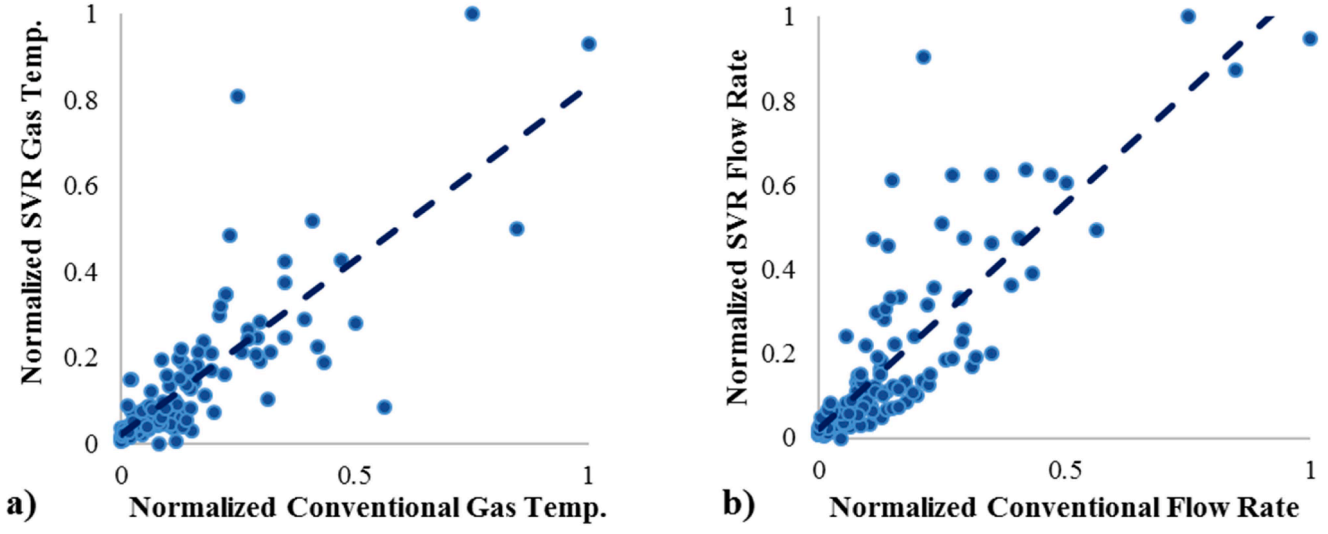


**Fig. 7.** The scatter plots of a) gas temperature, and b) molar flow rate in SVR vs. conventional states.

system. While these visualizations provide a qualitative understanding of temperature variations within the reactor, it is essential to elucidate their implications for catalyst activity, reaction kinetics, and product selectivity in $CH_4$ tri-reforming processes. Temperature gradients along the reactor bed play a crucial role in determining the performance and efficiency of catalysts employed in $CH_4$ tri-reforming reactions. Variations in temperature can influence the rates of individual reaction pathways, including steam reforming, partial oxidation, and dry reforming of methane, thereby impacting the overall conversion of $CH_4$ and the distribution of reaction products, including hydrogen, carbon monoxide, and carbon dioxide. High temperatures promote endothermic reactions such as steam reforming, which are favorable for hydrogen production but may also lead to catalyst deactivation due to sintering or carbon deposition. Conversely, lower temperatures favor exothermic reactions such as dry reforming, which are less susceptible to catalyst deactivation but may result in lower hydrogen yields and higher concentrations of by-products such as carbon monoxide and methane. Optimizing temperature profiles along the reactor bed is therefore essential for maximizing catalyst activity, product selectivity, and overall process efficiency in $CH_4$ tri-reforming processes. Strategies for thermal management may include adjusting the composition of the feed gas, modifying reactor operating conditions such as pressure and residence time, and implementing heat exchange systems to control temperature gradients within the reactor. Furthermore, the choice of catalyst formulation and reactor design can also influence temperature distribution and reaction kinetics in $CH_4$ tri-reforming processes. For example, catalysts with high thermal stability and resistance to carbon deposition may be preferred for operating at elevated temperatures, while reactor configurations that facilitate efficient heat transfer and temperature control can mitigate thermal gradients and enhance catalyst performance. In summary, temperature variations along the reactor bed have significant implications for catalyst activity, product selectivity, and overall process performance in $CH_4$ tri-reforming processes. By understanding and optimizing thermal management strategies, process engineers can enhance the efficiency, sustainability, and economic viability of membrane reactor systems for hydrogen production and synthesis gas generation.

Gas temperature distribution and molar flow rates are crucial parameters in membrane reactor systems, impacting reaction kinetics, product yields, and overall reactor performance. In this study, we investigated the distribution of these parameters along the reactor bed in conventional and membrane reactors for oxygen, water vapor, and carbon dioxide.

The scatter plot illustrates the gas temperature distribution along the reactor bed. As depicted, the gas temperature varies significantly along the reactor bed, indicating non-uniform heat transfer and thermal gradients within the system. Notably, higher temperatures are observed at the reactor inlet, gradually decreasing towards the outlet. This temperature profile suggests efficient heat utilization near the reactor inlet, potentially promoting favorable reaction kinetics, followed by heat dissipation along the reactor bed. The observed temperature distribution underscores the importance of thermal management in membrane reactor design. Effective heat transfer mechanisms, such as optimized reactor geometry and heat exchange surfaces, may be required to mitigate temperature gradients and ensure uniform temperature distribution. Such strategies can enhance reaction efficiency, minimize hotspots, and extend catalyst lifespan, thereby improving overall reactor performance.

Also, the molar flow rate distribution of chemical components along the reactor bed. The scatter plot reveals variations in molar flow rates, reflecting differences in reactant consumption, product formation, and mass transport phenomena along the reactor length. Notably, molar flow rates of individual components exhibit non-linear trends, indicative of complex reaction kinetics and mass transfer effects within the reactor. The observed distribution highlights the role of membrane permeability, chemical kinetics, and reactor design on molar flow rates. Variations in flow rates along the reactor bed underscore the need for precise control and optimization of operating conditions to maximize desired product yields while minimizing undesired by-products. Furthermore, insights from molar flow rate distribution can guide reactor design modifications, catalyst placement strategies, and flow distribution mechanisms to enhance reactor efficiency and selectivity.

The scatter plots depicting gas temperature and molar flow rate exhibit strong similarity and compatibility with results obtained using techniques employed in prior studies [30]. This alignment underscores the effectiveness and reliability of our experimental methods. Furthermore, our utilization of machine learning techniques has demonstrated commendable performance, effectively capturing and analyzing complex relationships within the data. The consistency observed between our findings and those of previous studies, coupled with the successful application of machine learning, validates the robustness of our approach and enhances confidence in the accuracy of our results.

According to Table 4, the SVR analysis demonstrates promising results for both gas temperature and molar flow rate prediction in comparison to conventional approaches. For gas temperature prediction, the SVR model achieves an RMSE of 2.15 °C in the SVR state, slightly lower than the 2.32 °C obtained in the conventional state. Additionally, the SVR model exhibits a higher coefficient of determination ($R^2$) of 0.87 in the SVR state compared to 0.82 in the conventional state, indicating a better fit of the SVR model to the data. Similarly, for molar flow rate prediction, the SVR model yields an RMSE of 0.027 mol/s in the SVR state, showing a marginal improvement over the 0.035 mol/s obtained in the conventional state. Moreover, the SVR model demonstrates a higher $R^2$ value of 0.95 in the SVR state compared to 0.91 in the conventional state, indicating a stronger correlation between the predicted and actual molar flow rates in the SVR model. These results suggest that the SVR approach offers a more accurate and reliable prediction of gas temperature and molar flow rate compared to conventional methods. The superior performance of the SVR model can be attributed to its ability to capture complex nonlinear relationships between input variables and output parameters, thereby enhancing predictive accuracy and model robustness. Furthermore, the SVR model's effectiveness in predicting gas temperature and molar flow rate has significant implications for reactor design and operation. Accurate temperature and flow rate predictions are crucial for optimizing reaction kinetics, catalyst performance, and overall process efficiency in $CH_4$ tri-reforming processes. By leveraging SVR-based predictive modeling, process engineers can enhance reactor design, control strategies, and process optimization techniques, leading to improved performance, sustainability, and economic viability of membrane reactor systems for hydrogen production and synthesis gas generation.

The obtained results offer valuable insights into the spatial distribution of gas temperature and molar flow rates in membrane reactor systems. Understanding these distributions is critical for optimizing reactor performance, improving product quality, and reducing energy consumption. Moving forward, future studies may focus on advanced computational modeling, experimental validation, and optimization techniques to refine reactor design, enhance process efficiency, and accelerate the transition towards sustainable and energy-efficient chemical processes.

**Table 4**
Comparison of performance metrics for gas temperature and molar flow rate between SVR and conventional states.

| Parameter | RMSE | | R2 | |
|---|---|---|---|---|
| | SVR | Conventional | SVR | Conventional |
| Gas Temperature | 2.15 | 2.32 | 0.87 | 0.82 |
| Molar Flow Rate | 0.027 | 0.035 | 0.95 | 0.91 |

### 3.8. Exploring limitations and future directions in membrane reactor research for $CH_4$ tri-reforming: a roadmap for advancement

While our study has made significant strides in elucidating the behavior of membrane reactors for $CH_4$ tri-reforming and synthesizing valuable insights into hydrogen yield optimization, several limitations and areas for future exploration warrant consideration.

One notable limitation is the reliance on computational simulations and mathematical models, which may not fully capture the intricacies of real-world reactor dynamics. Experimental validation of our findings through pilot-scale or lab-scale membrane reactor setups would enhance the robustness and applicability of our results. Furthermore, our investigation primarily focused on optimizing reactor parameters such as molar flow rates and membrane thickness to maximize hydrogen yield. Future studies could explore additional factors, such as catalyst composition, reactor geometry, and operating conditions, to further enhance reactor performance and efficiency.

Another area for future research is the investigation of long-term reactor stability and durability. While our study provides insights into short-term reactor behavior, understanding the effects of prolonged operation, catalyst degradation, and membrane fouling on performance is crucial for practical applications. Additionally, incorporating advanced machine learning techniques, such as deep learning algorithms, could offer more sophisticated modeling capabilities and predictive accuracy, further advancing the field of membrane reactor design and optimization. Interdisciplinary collaborations with experts in materials science, catalysis, and process engineering could facilitate the development of novel membrane materials, catalyst formulations, and reactor configurations tailored for specific synthesis gas production applications, paving the way for more efficient and sustainable energy conversion processes.

In conclusion, while our study represents a significant step forward in membrane reactor research through machine learning techniques, addressing the aforementioned limitations and pursuing avenues for future investigation will continue to drive innovation and progress in this field, ultimately contributing to the advancement of clean energy technologies.

## 4. Conclusion

The purpose of this study was to compare different feed configurations for a tri-reforming $CH_4$ reactor with a conventional reactor under ideal circumstances in order to generate appropriate synthesis gas for the methanol and Fischer–Tropsch synthesis processes, as well as direct dimethyl ether production. A microporous ceramic membrane was used for oxygen, vapor, and carbon dioxide distribution along the bed. A study was conducted to assess the impact of operational factors on reactor performance. The results showed that side feed influences the reaction route, resulting in variations in temperature and molar flow distribution across the reactor. The differential evolution algorithm was utilized to find optimal values for the ratios of $O_2/CH_4$, $H_2O/CH_4$, and $CO_2/CH_4$, membrane thickness, and shell pressure, with hydrogen yield selected as the objective function.

Optimization results show that the oxygen membrane reactor has the maximum hydrogen yield, reaching 2.02 and 1.75 for direct methanol synthesis and Fischer–Tropsch processes, respectively, among the examined structures. This reactor has increased hydrogen yield by 7.98 % and 10.03 % compared to the conventional tri-reforming reactor. Moreover, the elimination of hot spots within the catalyst bed is one of the advantages of using this reactor.

Also, this study shows that the CSA and SVR emerge as invaluable tools within our research framework, offering powerful capabilities for optimization and predictive modeling. The CSA, inspired by the brood parasitism of some cuckoo species, effectively navigates complex solution spaces to identify optimal parameters, ensuring the efficient optimization of membrane reactor structures. Its ability to balance exploration and exploitation enables the discovery of high-performing solutions, enhancing the overall effectiveness of our optimization process. Similarly, SVR, a versatile regression technique, proves instrumental in modeling the intricate relationships between input variables and hydrogen yield, facilitating accurate predictions within our study. By leveraging the unique strengths of CSA and SVR, our research benefits from robust optimization and predictive modeling methodologies, ultimately contributing to the advancement of membrane reactor design and synthesis gas production.

In conclusion, the use of the oxygen membrane reactor is more beneficial and feasible due to higher $CH_4$ conversion, increased hydrogen production, and longer catalyst lifespan compared to other structures for producing suitable synthesis gas for both processes. From an economic perspective, however, this reactor is considered the least favorable structure due to its higher shell pressure and membrane thickness. Nevertheless, it should be noted that while the conventional tri-reforming reactor has lower efficiency than the oxygen membrane reactor, its simpler design, not requiring a membrane, reduces initial and operational costs. Further comprehensive studies are recommended to examine the target process under optimal economic conditions in future research.

Future research in membrane reactor technology for $CH_4$ tri-reforming could focus on several key areas. Firstly, optimizing microporous ceramic membrane properties such as pore size distribution, surface area, and mechanical strength could enhance their performance in distributing oxygen, vapor, and carbon dioxide along the reactor bed. Advanced materials synthesis techniques could be employed for tailored membrane properties. Secondly, investigating novel catalytic materials with improved activity, selectivity, and stability in $CH_4$ tri-reforming reactions could significantly enhance reactor performance. Thirdly, exploring multifunctional reactor configurations integrating membrane technology with catalytic reactors, heat exchange systems, and process intensification techniques could offer enhanced performance, compactness, and energy efficiency. Fourthly, addressing the challenge of scaling up membrane reactor systems from laboratory-scale prototypes to industrial-scale production units through experimental validation and techno-economic analysis is crucial for commercialization. Lastly, exploring alternative process configurations like membrane-assisted tri-reforming or hybrid membrane-reactor systems could optimize overall process performance for hydrogen production and synthesis gas generation.

## CRediT authorship contribution statement

**Mohammadali Nasrabadi:** Methodology, Investigation, Formal analysis, Data curation. **Agus Dwi Anggono:** Software, Methodology, Investigation, Funding acquisition, Conceptualization. **Lidia Sergeevna Budovich:** Writing – original draft, Visualization, Validation, Formal analysis. **Sherzod Abdullaev:** Writing – review & editing, Software, Resources, Investigation. **Serikzhan Opakhai:** Visualization, Validation, Software, Resources.

## Declaration of competing interest

The authors declare that they have no known competing financial interests or personal relationships that could have appeared to influence the work reported in this paper.

## Data availability

Data will be made available on request.

## Acknowledgments

The authors would like to express their profound gratitude to the

Innovation and Research Centre and Faculty of Engineering at Universities Muhammadiyah Surakarta for their generous financial aid and steadfast support during the course of this research undertaking. The project's financial support was facilitated through the allocation of funds under contract numbers 231/A.3-III/FT/VI/2022.

## References

[1] H. Eslami, H. Yousefyani, M. Yavary Nia, et al., On how defining and measuring a channel bed elevation impacts key quantities in sediment overloading with supercritical flow, Acta Geophys. 70 (2022) 2511–2528.
[2] F. Shacheri, N.S.R. Nikou, A.N. Ziaei, M. Saeedi, Surface dense discharge from rectangular and trapezoidal channels, Flow Meas. Instrum. 87 (2018) 102213.
[3] T. Taner, The micro-scale modeling by experimental study in PEM fuel cell, J. Therm. Eng. 3 (6) (2017) 1515–1526.
[4] T. Taner, S.A.H. Naqvi, M. Ozkaymak, Techno-economic analysis of a more efficient hydrogen generation system prototype: a case study of PEM electrolyzer with Cr-C coated SS304 bipolar plates, Fuel Cells 19 (1) (2019) 19–26.
[5] S.A.H. Naqvi, et al., Hydrogen production through alkaline electrolyzers: a techno-economic and enviro-economic analysis, Chem. Eng. Technol. 46 (3) (2023) 474–481.
[6] S.-H. Lee, et al., Tri-reforming of CH4 using CO2 for production of synthesis gas to dimethyl ether, Catal. Today 87 (1–4) (2003) 133–137.
[7] Q. Zhao, et al., Steam reforming of CH4 at low temperature on Ni/ZrO2 catalyst: effect of H2O/CH4 ratio on carbon deposition, Int. J. Hydrogen Energy 45 (28) (2020) 14281–14292.
[8] H. Gruber, et al., Fischer-Tropsch products from biomass-derived syngas and renewable hydrogen, BioMass Convers. Biorefin. 11 (2021) 2281–2292.
[9] H. Chen, F. Dong, S.D. Minteer, The progress and outlook of bioelectrocatalysis for the production of chemicals, fuels and materials, Nat. Catal. 3 (3) (2020) 225–244.
[10] L. Chen, P. Gangadharan, H.H. Lou, Sustainability assessment of combined steam and dry reforming versus tri-reforming of methane for syngas production, Asia Pac. J. Chem. Eng. 13 (2) (2018) e2168.
[11] W. Wei, et al., Energy consumption and greenhouse gas emissions of high-carbon ferrochrome production, JOM 75 (4) (2023) 1206–1220.
[12] R. Gao, et al., Sustainable production of methanol using landfill gas via carbon dioxide reforming and hydrogenation: process development and techno-economic analysis, J. Clean. Prod. 272 (2020) 122552.
[13] O.U. Osazuwa, S.Z. Abidin, An overview on the role of lanthanide series (rare earth metals) in H2 and syngas production from CH4 reforming processes, Chem. Eng. Sci. 227 (2020) 115863.
[14] V.V. Thyssen, et al., Syngas production via methane tri-reforming on Ni/La2O3–αAl2O3 catalysts, Braz. J. Chem. Eng. (2023) 1–13.
[15] E.S.K. Why, et al., Single-step catalytic deoxygenation of palm feedstocks for the production of sustainable bio-jet fuel, Energy 239 (2022) 122017.
[16] J. Xu, W. Lin, Integrated hydrogen liquefaction processes with LNG production by two-stage helium reverse Brayton cycles taking industrial by-products as feedstock gas, Energy 227 (2021) 120443.
[17] H. Du, et al., Activity and selectivity enhancement of silica supported cobalt catalyst for alcohols production from syngas via Fischer-Tropsch synthesis, Int. J. Hydrogen Energy 47 (7) (2022) 4559–4567.
[18] A.A. Markov, O.V. Merkulov, A.Y. Suntsov, Development of membrane reactor coupling hydrogen and syngas production, Membranes 13 (7) (2023) 626.
[19] S.-J. Kim, et al., Thin hydrogen-selective SAPO-34 zeolite membranes for enhanced conversion and selectivity in propane dehydrogenation membrane reactors, Chem. Mater. 28 (12) (2016) 4397–4402.
[20] V.S. Aslamova, et al., Automated Thermal Design of Reactor For Producing Sulfur-Containing Sorbent in Heating Reaction Mixture, Vestnik of Astrakhan State Technical University. Series: Management, Computer Sciences and Informatics, 2023, pp. 7–15.
[21] M. Bouyahyi, et al., In-reactor polypropylene functionalization- the influence of catalyst structures and reaction conditions on the catalytic performance, Macromolecules 55 (3) (2022) 776–787.
[22] M. Osat, F. Shojaati, A. Hafizi, Optimization and improvement of a conventional tri-reforming reactor to an energy efficient membrane reactor for hydrogen production, Chem. Eng. Process.-Process Intensif. 175 (2022) 108933.
[23] R.C. Sabioni, J. Daaboul, J.Le Duigou, Joint optimization of product configuration and process planning in reconfigurable manufacturing systems, Int. J. Ind. Eng. Manage. 13 (1) (2022) 58–75.
[24] D.A. Kurniady, et al., Construction project progress evaluation using a quantitative approach by considering time, cost and quality, Int. J. Ind. Eng. Manage. 13 (1) (2022) 49–57.
[25] Y. Alaiwi, et al., Simulation and investigation of bioethanol production considering energetic and economic considerations, Int. J. Low-Carbon Technol. 18 (2023) 191–203.
[26] W. Gao, et al., Optimizing N application for forage sorghum to maximize yield, quality, and N use efficiency while reducing environmental costs, Agronomy 12 (12) (2022) 2969.
[27] D.L. Bjelica, et al., Relationship between project success factors, project success criteria and project success in SME: evidence from selected European transitional economies, Int. J. Ind. Eng. Manage. 14 (4) (2023) 297–310.
[28] Y. Alaiwi, A. Taha, Y. ALjumaili, Enhancement of the polycrystalline solar panel performance using a heatsink cooling system with PCM, Int. J. Eng. Artif. Intell. 4 (2023) 24–34.
[29] M. Sakbodin, et al., Direct nonoxidative methane conversion in an autothermal hydrogen-permeable membrane reactor, Adv. Energy Mater. 11 (46) (2021) 2102782.
[30] A. Alipour-Dehkordi, M.H. Khademi, O2, H2O or CO2 side-feeding policy in methane tri-reforming reactor: the role of influencing parameters, Int. J. Hydrogen Energy 45 (30) (2020) 15239–15253.
[31] R. Franz, E.A. Uslamin, E.A. Pidko, Challenges for the utilization of methane as a chemical feedstock, Mendeleev Commun. 31 (5) (2021) 584–592.
[32] S. Abdullaev, et al., A novel model of a hydrogen production in micro reactor: conversion reaction of methane with water vapor and catalytic, Int. J. Thermofluids 20 (2023) 100510.
[33] P. Yan, Y. Cheng, Foam structured membrane reactor for distributed hydrogen production, J. Memb. Sci. 661 (2022) 120927.
[34] W. Liang, et al., Stable Ce0. 8Gd0. 2O2-δ oxygen transport membrane reactor for hydrogen production, Appl. Catal. A: General 650 (2023) 118980.
[35] R.N. Ewuzie, J.R. Genza, A.Z. Abdullah, Review of the application of bimetallic catalysts coupled with internal hydrogen donor for catalytic hydrogenolysis of lignin to produce phenolic fine chemicals, Int. J. Biol. Macromol. (2024) 131084.
[36] M. Ishaq, I. Dincer, Development of a new renewable energy system for clean hydrogen and ethanol production, Energy Convers. Manage. 306 (2024) 118304.
[37] M. Rezaei, M. Sameti, F. Nasiri, Design optimization of an integrated tri-generation of heat, electricity, and hydrogen powered by biomass for cold climates, Inte. J. Thermofluids (2024) 100618.
[38] L.G. Aguiar, A.F. Siqueira, Modeling of catalyst deactivation in humic acid degradation, Ind. Eng. Chem. Res. 61 (25) (2022) 8708–8713.
[39] S. Sakamoto, T. Matsuoka, Y. Nakamura, Effective thermal design concept of Sabatier reactor by controlling catalyst distribution profile, Catal. Letters 150 (2020) 2928–2936.
[40] J.A. Torres, et al., Role of Cu0-TiO2 interaction in catalyst stability in CO2 photoreduction process, J. Environ. Chem. Eng. 10 (2) (2022) 107291.
[41] H.B. Bacha, et al., A comprehensive review on nanofluids: synthesis, cutting-edge applications, and future prospects, Int. J. Thermofluids (2024) 100595.
[42] Z. Liu, et al., Recent progress on microbial electrosynthesis reactor designs and strategies to enhance the reactor performance, Biochem. Eng. J. 190 (2023) 108745.
[43] H.O. Mohamed, et al., Isolating the effect of Co and Ce on Ni–X–Y/Al2O3 bi-and trimetallic reforming catalysts for hydrogen generation, Int. J. Hydrogen Energy 51 (2024) 922–935.
[44] X. Zhuang, et al., Numerical investigation of a multichannel reactor for syngas production by methanol steam reforming at various operating conditions, Int. J. Hydrogen Energy 45 (29) (2020) 14790–14805.
[45] S. Paul, et al., Computational investigation of cross flow heat exchanger: a study for performance enhancement using spherical dimples on fin surface, Int. J. Thermofluids 20 (2023) 100483.
[46] E.M. de Medeiros, et al., Production of ethanol fuel via syngas fermentation: optimization of economic performance and energy efficiency, Chem. Eng. Sci.: X 5 (2020) 100056.
[47] Z.A. Aboosadi, A. Jahanmiri, M. Rahimpour, Optimization of tri-reformer reactor to produce synthesis gas for methanol production using differential evolution (DE) method, Appl. Energy 88 (8) (2011) 2691–2701.
[48] S. Khajeh, Z.A. Aboosadi, B. Honarvar, A comparative study between operability of fluidized-bed and fixed-bed reactors to produce synthesis gas through tri-reforming, J. Nat. Gas Sci. Eng. 19 (2014) 152–160.
[49] J. Xu, G.F. Froment, Methane steam reforming, methanation and water-gas shift: I. Intrinsic kinetics, AIChE J. 35 (1) (1989) 88–96.
[50] D.L. Trimm, C.-W. Lam, The combustion of methane on platinum—alumina fibre catalysts—I: kinetics and mechanism, Chem. Eng. Sci. 35 (6) (1980) 1405–1413.
[51] C. De Smet, et al., Design of adiabatic fixed-bed reactors for the partial oxidation of methane to synthesis gas. Application to production of methanol and hydrogen-for-fuel-cells, Chem. Eng. Sci. 56 (16) (2001) 4849–4861.
[52] A. Alipour-Dehkordi, M.H. Khademi, Use of a micro-porous membrane multi-tubular fixed-bed reactor for tri-reforming of methane to syngas: CO2, H2O or O2 side-feeding, Int. J. Hydrogen Energy 44 (60) (2019) 32066–32079.
[53] B. Weigand, Analytical Methods For Heat Transfer and Fluid Flow Problems, 263, Springer, 2004.
[54] J.P. Holman, Heat Transfer, McGraw Hill Higher Education, 2010.
[55] K. Gosiewski, et al., Effect of the intraparticle mass transport limitations on temperature profiles and catalytic performance of the reverse-flow reactor for the partial oxidation of methane to synthesis gas, Chem. Eng. Sci. 54 (20) (1999) 4589–4602.
[56] H.S. Fogler, Elements of Chemical Reaction Engineering, Pearson Educacion, 1999.
[57] M.L. Rodriguez, et al., Oxidative dehydrogenation of ethane to ethylene in a membrane reactor: a theoretical study, Catal. Today 157 (1–4) (2010) 303–309.
[58] P. Uchytil, O. Schramm, A. Seidel-Morgenstern, Influence of the transport direction on gas permeation in two-layer ceramic membranes, J. Memb. Sci. 170 (2) (2000) 215–224.
[59] W. Zhang, et al., Discrete optimization algorithm for optimal design of a solar/wind/battery hybrid energy conversion scheme, Int. J. Low-Carbon Technol. 16 (2) (2021) 326–340.
[60] B. Du, et al., State-of-charge estimation for second-life lithium-ion batteries based on cell difference model and adaptive fading unscented Kalman filter algorithm, Int. J. Low-Carbon Technol. 16 (3) (2021) 927–939.
[61] C. Kang, et al., A 1D linearization–based MILP–NLP method for short-term hydrothermal operation, Int. J. Low-Carbon Technol. 17 (2022) 540–549.
[62] M. MUNRO, Evaluated material properties for a sintered alpha-alumina, J. Am. Ceram. Soc. 80 (8) (1997) 1919–1928.

[63] B. Novakovic, M. Kashkoush, Modeling the matching stage of HDPE hot plate welding: a study using regression and support vector machine models, Polym. Eng. Sci. 64 (2) (2024) 827–844.
[64] V.V. Belikov, I.A. Prokuronov, Password strength verification based on machine learning algorithms and LSTM recurrent neural networks, Russ. Technol. J. 11 (4) (2023) 7–15.
[65] J.S. Kang, et al., Nickel-based tri-reforming catalyst for the production of synthesis gas, Appl. Catal. A: General 332 (1) (2007) 153–158.
[66] Y. Zhang, et al., A novel tubular oxygen-permeable membrane reactor for partial oxidation of CH4 in coke oven gas to syngas, Int. J. Hydrogen Energy 38 (21) (2013) 8783–8789.
[67] X. Pang, et al., Membrane reactors accelerate polymer photosensitizer-based singlet oxygen reactions, Chem. Eng. J. 433 (2022) 134444.
[68] Q. He, et al., Electrochemical hydrogen-storage capacity of graphene can achieve a carbon-hydrogen atomic ratio of 1: 1, Sci. China Chem. (2022) 1–4.